Supplementary Information

EXPERIMENTAL PRESERVATION OF MUSCLE TISSUE IN QUARTZ SAND AND KAOLINITE

SHARON A. NEWMAN[1,2*], MIRNA DAYE[1], SIRINE C. FAKRA[3], MATTHEW A. MARCUS[3], MIHKEL PAJUSALU[1], SARA B. PRUSS[4], EMILY F. SMITH[5] AND TANJA BOSAK[1]

[1]*Department of Earth, Atmospheric and Planetary Sciences, Massachusetts Institute of Technology, Cambridge, Massachusetts 02139, USA*

[2]*Division of Geological and Planetary Sciences, California Institute of Technology, Pasadena, California 91125, USA*

[3]*Advanced Light Source, Lawrence Berkeley National Laboratory, Berkeley, California 94720, USA*

[4]*Department of Geosciences, Smith College, Northampton, Massachusetts 01063, USA*

[5]*Department of Earth and Planetary Sciences, Johns Hopkins University, Baltimore, Maryland 21218, USA*

email: snewman@caltech.edu

SUPPLEMENTARY METHODS

Carbon-Hydrogen-Nitrogen Analyses

To prep samples for carbon-hydrogen-nitrogen (CNH) analyses, a mm-sized section of tissue was dried under vacuum for 48 hours at room temperature. Triplicate subsamples were analyzed of muscles that had not been incubated in kaolinite/sand (two specimens), muscles that were exhumed from kaolinite after 45 days (two specimens) and a single muscle that was exhumed from quartz sand after 45 days. Results were reported as percent weight of each element.

Due to the small number of exhumed muscles, each mm-sized section of tissue was measured separately and considered to be an independent sample. Gaussian distributions were identified by creating quantile-quantile plots of carbon, hydrogen and nitrogen contents (Supplementary Fig. 5); slight deviations from normal distributions were assumed to result from the small sample size, rather than failure of the data to fit Gaussian curves. We performed Welch two-sample t-tests to determine differences in elemental composition (CHN) between samples incubated in kaolinite and those analyzed before incubation. Muscles incubated in quartz sand were excluded from these analyses because only one sample was successfully recovered during experimentation. Corrections for multiple hypothesis testing were made using Bonferroni post hoc analyses ($\alpha = 0.05/n$, where α = significance level and $n = 3$, the number of hypotheses). All statistical tests were conducted using the statistical software package R (version 3.4.4).

Electron Microscopy

Scanning Electron Microscopy.–Muscles were imaged by scanning electron microscopy with energy dispersive X-ray spectroscopy (SEM-EDS) to determine the presence and distribution of elements in the mineral veneers that coated and/or impregnated muscle tissues. Pieces of exhumed muscles (~2 cm wide) were separated using a 1 mL plastic pipette tip. Samples for SEM were fixed in 2.5% glutaraldehyde in 0.1 M sodium cacodylate buffer with 0.1% $CaCl_2*H_2O$ (pH = 7.4) and stored for three to seven days at 4˚C to ensure the complete fixation of tissues. Fixed samples were rinsed twice for 10 min with a 0.1 mM sodium cacodylate buffer solution (stored at 4˚C), followed by 6 rinses with double distilled water. Samples were dehydrated using an ethanol-water drying series (30%, 50%, 70%, 80%, 90%, 100%, 100%, 100%) in successive 20 min steps and left overnight to dry. Dehydrated muscle tissues were transferred to carbon tape and coated with gold and palladium to reduce SEM image charging (Keck Facility, Whitehead Institute, MIT, Cambridge, MA, USA). All samples were imaged on a Zeiss Supra Scanning Electron Microscope with a secondary electron detector (Center for Nanoscale Systems, Harvard University, Cambridge, MA, USA). Elemental composition in regions of interest was determined using an electron-dispersive X-ray spectrometer operating at 10-13 kV.

Transmission Electron Microscopy.–Samples were imaged by transmission electron microscopy (TEM) to determine the mineral composition of the veneers. To prepare select samples for TEM analyses, pre-frozen muscles (-80˚C) were partially thawed at room temperature for 5 to 10 min and small pieces (~2 mm wide) were separated using a sterile plastic pipette tip. These subsamples were placed in a 1.7 mL microcentrifuge tube (VWR International, Radnor, PA, USA), suspended in filter-sterilized double distilled water (Arodisc® Syringe

Filters with Supor® Membrane, Pall Laboratory, Port Washington, NY, USA) and shaken by hand for 30 s. Two microliters of the suspended solution was placed on an LC-200 grid (Electron Microscopy Sciences, Cat # LC-200-Cu, Hatfield, PA, USA) and imaged with a JEOL 2010F transmission electron microscope (TEM, JEOL 2010F, JEOL, Peabody, MA, USA). Gold standard was used as a reference for SAED determination of the sample. The high-angle annular dark-field detector (Gatan HAADF, Pleasanton, CA, USA) for atomic resolution scanning electron transmission microscopy in free-lens control mode (STEM) and energy dispersive spectrometer (EDS, Bruker silicon drift detector SDD, Billerica, MA, USA) enabled elemental analysis at nanoscale resolution. Images were taken using a digital camera (Gatan Orius, Pleasanton, CA, USA) for TEM and STEM mode. SAED patterns were imaged using Gatan digiscan unit and TEM, STEM and SAED images were recorded and treated using Gatan digital micrograph software. EDS spectra were recorded and treated using the INCA software program (Oxford instruments, Abingdon, UK).

Synchrotron-Based Analyses

X-Ray Microprobe.–The distribution and speciation of iron in mineral veneers was identified at the Advanced Light Source beamline 10.3.2 (Marcus et al., 2004) (Lawrence Berkeley National Laboratory, Berkeley, CA, USA). Pre-frozen samples (-80˚C) were first thawed, air dried and then mounted on the non-sticky side of Kapton® polyimide tape (DuPont, Hayward CA, USA) for analysis. Micro-focused X-ray fluorescence (μXRF) maps of muscles before incubation and samples exhumed from kaolinite and quartz sand were acquired using an incident beam at 100eV above the iron K-edge; spots of interest were selected for iron K-edge X-ray absorption near edge structure (μXANES) spectroscopy measurements. The XANES spectra

were acquired in five representative spots on each sample and sterile kaolinite grains were also measured. X-ray fluorescence emission data were recorded using a seven-element germanium (Ge) solid state detector (Canberra, ON, Canada) for S, Fe, Ca, K, Cl, Si, Al and P. XANES spectra were calibrated with an iron foil (first derivative maximum set at 7110.75 eV). Maps were recorded with a beam spot size of 6 x 6 µm and spectra were recorded with a beam spot size of 12 x 3 µm. Maps were deadtime-corrected and decontaminated. All spectra were deadtime-corrected, calibrated, pre-edge background subtracted and post-edge normalized using a suite of LabVIEW based custom programs available at the beamline following procedures described in Marcus et al. (2008). Spectra recorded on various spots were averaged in Athena (Demeter 0.9.24, Ravel and Newville, 2005). Individual and averaged spectra were least-square fitted as a linear combination of spectra from the large database of iron-bearing standard compounds (Marcus et al., 2008 and the updated 10.3.2 database). Two-dimensional plots of iron XANES data were generated according to general methods described in Marcus et al. (2008) and a Matlab code described elsewhere (Fakra, 2015). This code is available at the beamline.

Micro-X-Ray Diffraction.–The composition of the sterile sediments was determined at the Advanced Light Source (beamline 12.3.2, Berkeley, CA, USA) using a combination of micro-X-ray fluorescence (µXRD) mapping and micro-X-ray diffraction (µXRD) at 10 keV. Previously frozen samples were thawed, but not dried and placed on the sticky side of Kapton® polyimide tape (DuPont, Hayward CA, USA) for analysis. A 3 x 3 µm XRF map was first generated and points with high iron intensity were selected for diffraction. XRD data was converted to 2D powder diffractions using the computer program available at the beamline (XRDSol2) and minerals were identified using the computer program HighScore Plus.

Water Chemistry

Oxygen.–Dissolved oxygen concentrations were measured on days 10, 30 and 45 by injecting known volumes of samples collected either from the porewater or from the water column with a syringe into 60 mL serum bottles and measuring oxygen partial pressure change in the headspace. The bottles were previously flushed with oxygen free nitrogen and oxygen diffused out of the samples in less than 20 minutes. Oxygen partial pressure was measured by detecting changes in the fluorescence lifetime of palladium(II)-5,10,15,20-tetrakis-(2,3,4,5,6-pentafluorphenyl)-porphyrin (Pd-TFPP) (Lehner et al., 2015) using an in-house built fluorescence lifetime sensor (Pajusalu et al., 2018). Triplicate measurements of each porewater/water column sample were made to ensure the accuracy of each oxygen reading. Due to unexpectedly large oxygen absorption rates of the reductive compounds in the sample, the dissolved concentrations underestimate the actual oxygen concentrations.

Colorimetric Assays.–Porewater samples from kaolinite and sand were collected using 5 mL plastic syringes with 18 gauge needles (VWR International, Radnor, PA, USA). The needle tips were inserted ~6.5 cm below the surface of the substrate on days 10, 15, 30 and 45 to measure iron and sulfide and on days 10, 20, 30 and 45 to measure dissolved silica. All samples were centrifuged aerobically for 10 minutes at 10,000 rotations per minute to separate the particulate matter from the liquid medium. The supernatant was decanted and filtered aerobically through 0.2 µm sterile syringe filters with polyethersulfone membranes (Acrodisc®, Pall Laboratory, Westborough, MA, USA). Triplicate measurements were made for each sample and

the average of these was used as a final value. Sterile medium that lacked iron was also measured and used for background subtraction.

Iron.–Following the methods of Stookey (1970) for Fe(II) and Fe(III) determination, 100 µL of ferrozine reagent (3-(2-pyridyl)-5,6-bis(4-phenylsulfonic acid)-1,2,4-triazine, Aldrich #160601, prepared in 1.0 M ammonium acetate solution, CH_3COONH_4, Aldrich #372331) was added to one mL of experimental sample and stored at -4˚C until analyzed. Standards were prepared from stock solutions of 2.02 mM of $FeCl_2*4H_2O$ that was diluted with 0.1 M solution of NaCl and a previously prepared 6.16 mM $FeCl_3$ reagent that was prepared from anhydrous ferric chloride (Aldrich #157740). The stock solutions were diluted with double distilled water and acidified with 2% HCl by volume. Total iron was determined by reducing Fe(III) in the samples and standards to Fe(II) by adding 150 µL of 1.4 M hydroxalamine hydrochloride ($H_2NOH.HCl$, Aldrich # 379921) and 50 µL of 10 M ammonium acetate to 800 µL of sample/standard. The concentration of Fe(III) was calculated by subtracting the previously determined concentration of Fe(II) from the total iron concentration in the same sample. The following standard dilution series were analyzed together with the experimental samples: 0, 0.001, 0.002, 0.005, 0.025, 0.035, 0.050 and 0.101 mM of Fe(II) and 0, 0.001, 0.003, 0.006, 0.031, 0.062, 0.074, 0.092, 0.111 and 0.123 mM of Fe(III).

Several porewater samples exceeded the saturation limit for measurement and were diluted 20x with 0.1 M NaCl water after the addition of ferrozine (Supplementary Table 2). The effect of sample dilution on the measurements was determined by assaying the following standard dilution series that was diluted 20x with a 0.1 M NaCl solution after the addition of ferrozine: 0, 0.151, 0.302, 0.754, 1.21, 1.51 and 2.01 mM of Fe(II). Measurements of undiluted

and diluted samples from the same experiments and time points were compared when possible. Dilution had little to no effect on the measured concentration of Fe(II) if the original sample/standard contained less than 0.75 mM of Fe(II) (Supplementary Fig. 6). However, the assay consistently underestimated the concentrations of total iron when samples were diluted after the addition of ferrozine and the concentration of Fe(II) in samples/standards that contained higher concentrations of Fe(II) (Supplementary Fig. 6). Thus, all measurements of Fe(III) concentrations in samples that were diluted after the addition of ferrozine are lower bounds.

Silica.–Silica concentrations were determined following the methods described in Newman et al. (2017). To determine the concentrations of dissolved silica, filtered and frozen samples that had been stored at -20˚C in tightly capped 15 mL conical centrifuge tubes were left at room temperature until the liquid had completely thawed. Samples were diluted 10x in a silica-free, sterile medium. Two standard dilution series were prepared using a concentrated silica standard (J.T. Baker "Dilut-IT" silica standard, 16.64 mM) and added to the silica-free medium: (1) 0, 0.02, 0.04, 0.08, 0.10, 0.21, 0.42 and (2) 0, 0.21, 0.42, 0.83, 1.04, 2.08, 4.16 mM. Silica standards were also diluted 10 times. Potential contamination by silica from the syringe filters (0.2 µm, Acrodisc®, Pall Laboratory, Westborough, MA, USA) and needles (VWR International, Radnor, PA, USA) was determined to be negligible.

Sulfide.–The concentration of dissolved S(-II) species (H_2S, HS^- and S_2^-) were determined by adding one mL of 0.05 M zinc acetate ($Zn(CH_3COO)_2 \cdot 2H_2O$, Aldrich #383058, prepared in double distilled water) to 200 µL of sample, using the modified method of Cline (1969). Samples were stored at 4˚C until measurement. The 0.1 M stock solution of Na_2S was

prepared by adding 0.1 M of sodium sulfide nonahydrate ($Na_2S \cdot 9H_2O$, Aldrich #431648) to anaerobic double distilled water that had been allowed to boil at 100˚C. The solution was transferred to a hermetically sealed container and the headspace of this bottle was flushed with CO_2:N_2 (20:80, v/v) using standard anaerobic techniques. Standards were prepared by diluting 100 mM Na_2S with 0.05 M zinc acetate (to 0.005, 0.010, 0.020, 0.050 and 0.100 mM concentrations). Before the colorimetric assay, 40 µL of diamine reagent was added to all samples and standards. This reagent included 1.6 g N,N dimethyl-p-phenyldiamine sulfate salt, $(CH_3)_2NC_6H_4NH_2 \cdot H_2SO_4$, Aldrich #186384) and 4 g of anhydrous ferric chloride (Aldrich #157740) dissolved in 100 ml of 6 N hydrochloric acid.

Saturation Indices.–The degree of solution saturation state with respect to each mineral phase dissolution/precipitation reaction is expressed in terms of the Gibbs free energy of reaction, ΔG_r

$$\Delta G_r = RT \ln[IAP/Keq] = RT \ln[\Omega]$$

where R is the gas constant, T is the absolute temperature (K), IAP and K_{eq} are the ion activity product and the equilibrium constant, respectively and Ω = IAP/ Keq. To calculate the saturation indices (SI) of different mineral phases, we used the geochemical computer program PHREEQC Version 1.6 (Parkhurst and Appelo, 1999). For input information, we used chemical and physical concentrations for each experimental condition. We did not measure aluminum concentrations in the pore fluids and used an assumed value of 0.1 µM (Mackin and Aller, 1986).

REFERENCES

CLINE, J.D., 1969, Spectrophotometric determination of hydrogen sulfide in natural waters: Limnology and Oceanography, v. 14, p. 454–458, doi: 10.4319/lo.1969.14.3.0454.

FAKRA, S.C., 2015, Spectro-microscopic studies of microbial selenium and iron reduction in a metal contaminated aquifer: Unpublished Ph.D. thesis, University of California, Berkeley, 145 p.

LEHNER, P., LARNDORFER, C., GARCIA-ROBLEDO, E., LARSEN, M., BORISOV, S.M., REVSBECH, N.-P., GLUD, R.N., CANFIELD, D.E. and KLIMANT, I., 2015, LUMOS - A sensitive and reliable optode system for measuring dissolved oxygen in the nanomolar range: PLoS ONE, v. 10, e0128125, doi: 10.1371/journal.pone.0128125.

MACKIN, J.E., and ALLER, R.C., 1986, The effects of clay mineral reactions on dissolved Al distributions in sediments and waters of the Amazon continental shelf: Continental Shelf Research, v. 6, p. 245–262, doi: 10.1016/0278-4343(86)90063-4.

MARCUS, M.A., MACDOWELL, A.A., CELESTRE, R., MANCEAU, A., MILLER, T., PADMORE, H.A., and SUBLETT, R.E., 2004, Beamline 10.3.2 at ALS: A hard X-ray microprobe for environmental and materials sciences: Journal of Synchrotron Radiation, v. 11, p. 239–247, doi: 10.1107/S0909049504005837.

MARCUS, M.A., WESTPHAL, A.J., and FAKRA, S.C., 2008, Classification of Fe-bearing species from K-edge XANES data using two-parameter correlation plots: Journal of Synchrotron Radiation, v. 15, p. 463–468, doi: 10.1107/S0909049508018293.

NEWMAN, S.A., KLEPAC-CERAJ, V., MARIOTTI, G., PRUSS, S.B., WATSON, N., and BOSAK, T., 2017, Experimental fossilization of mat-forming cyanobacteria in coarse-grained siliciclastic sediments: Geobiology, v. 15, p. 484–498, doi: 10.1111/gbi.12229.

PAJUSALU, M., BORLINA, C.S., SEAGER, S., ONO, S., and BOSAK, T., 2018, Open-source sensor for measuring oxygen partial pressures below 100 microbars: PLoS ONE, v. 13, e0206678, doi: 10.1371/journal.pone.0206678.

PARKHURST, D.L., and APPELO, C.A.J., 1999, User's guide to PHREEQC (version 2) - A computer program for speciation, batch-reaction, one-dimensional transport, and inverse geochemical calculations: U.S. Geological Survey, 312 p.

RAVEL, B., and NEWVILLE, M., 2005, ATHENA, ARTEMIS, HEPHAESTUS: Data analysis for X-ray absorption spectroscopy using IFEFFIT: Journal of Synchrotron Radiation, v. 12, p. 537–541, doi: 10.1107/S0909049505012719.

STOOKEY, L.L., 1970, Ferrozine-A new spectrophotometric reagent for iron: Analytical Chemistry, v. 42, p. 779–781, doi: 10.1021/ac60289a016.

SUPPLEMENTARY RESULTS

Oxygen

Dissolved oxygen values were determined for pore fluids (~6.5 cm below the sand/clay surfaces) and water columns (~3 cm above the sand/clay surfaces) (Supplementary Fig. 1). Values for dissolved oxygen in the porewaters were less than or equal to 8.1 ± 2.8 µM. Dissolved oxygen values in the water column ranged from 20.4 ± 12.9 to 40.8 ± 10.9 µM on day 10, 19.1 ± 2.3 to 60.3 ± 6.0 µM on day 30 and 32.0 ± 5.7 to 63.8 ± 15.7 µM on day 45. The observed increase in dissolved oxygen concentrations between 30 and 45 days likely reflects the removal of the decaying organic material during the medium replacement and the decreasing amounts of dissolved organic matter and organic decay after day 30.

Micro-X-Ray Diffraction

Micro-X-ray diffraction (μXRD) of the sterile substrates in the absence of muscle tissues demonstrated that sand contained albite, clintonite, gismondine, wüstite, hematite, phlogopite, quartz and saponite (Supplementary Fig. 4A). Sterile kaolinite substrates contained kaolinite grains, as well as natural impurities such as muscovite, brookite and a lead-rich mineral (possibly hinsdalite) (Supplementary Fig. 4B, see Supplementary Fig. 7). Missing major peaks resulting from grain orientation during μXRD analyses hindered the identification of some minerals in the sterile substrates.

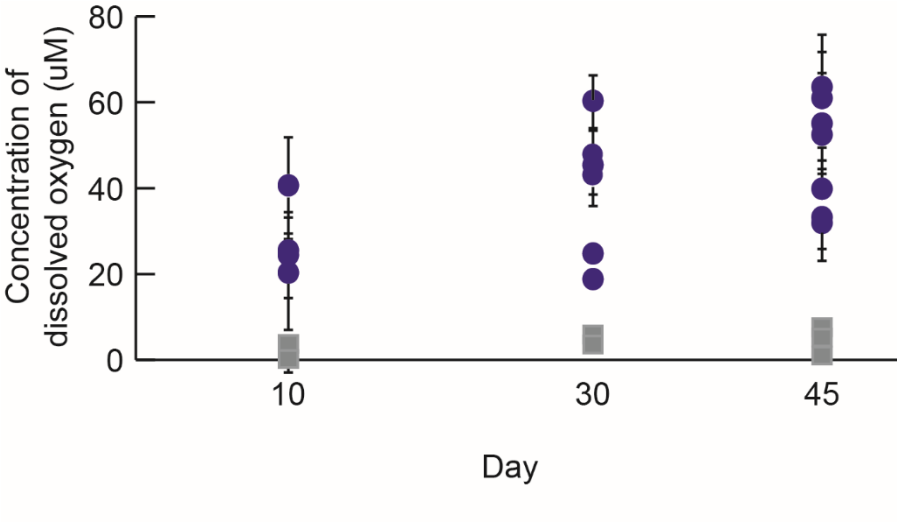

SUPPLEMENTARY FIGURE 1.–Concentrations of dissolved oxygen (µM) on days 10, 30 and 45 after tissue burial. Error bars are shown for triplicate measurements. Purple circles = water column values; gray squares = porewater values.

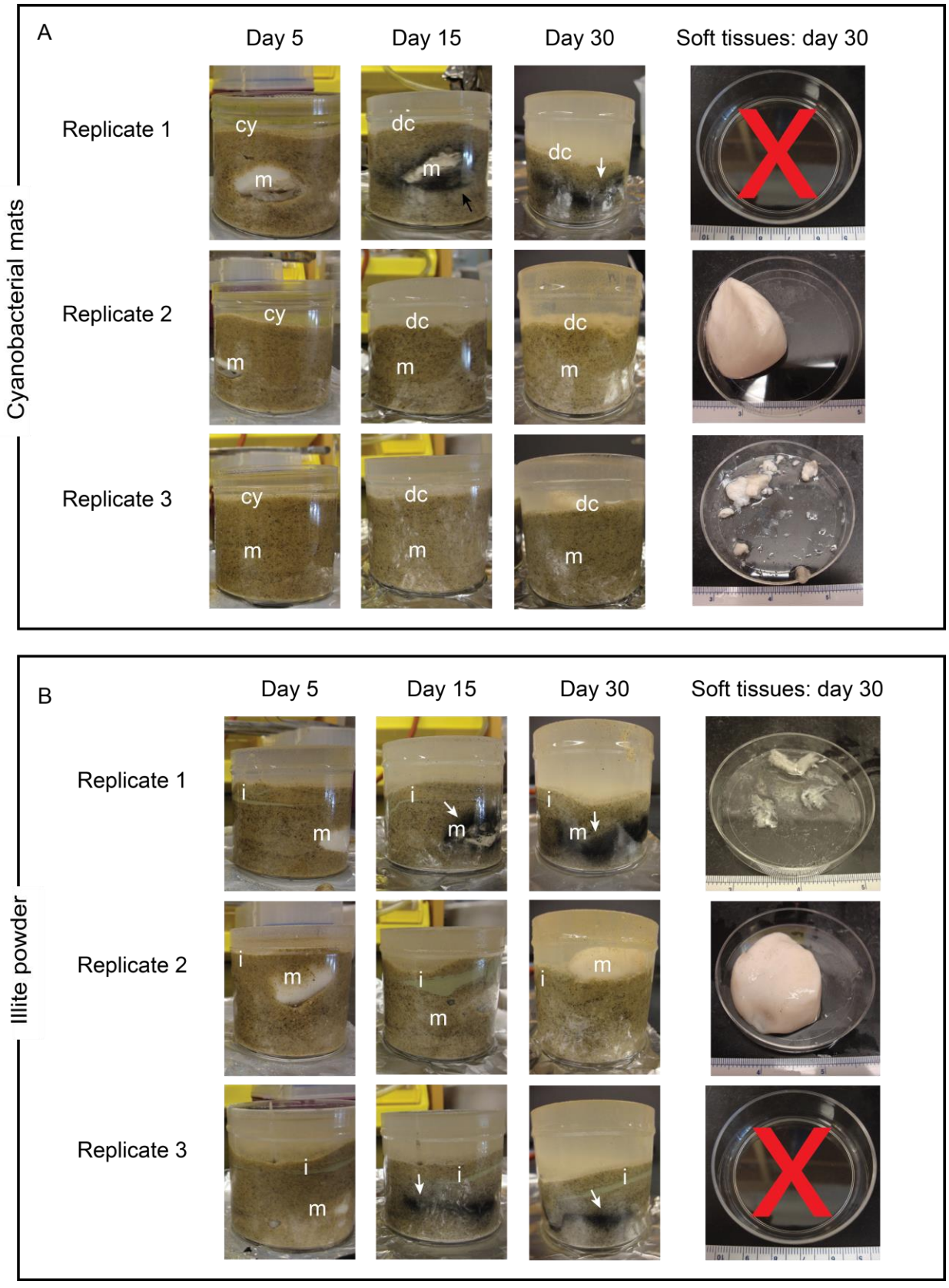
A
Day 5
Day 15
Day 30
Soft tissues: day 30
Cyanobacterial mats
Replicate 1
Replicate 2
Replicate 3
cy
m
dc
m
dc
m
B
Day 5
Day 15
Day 30
Soft tissues: day 30
Illite powder
Replicate 1
Replicate 2
Replicate 3
i
m

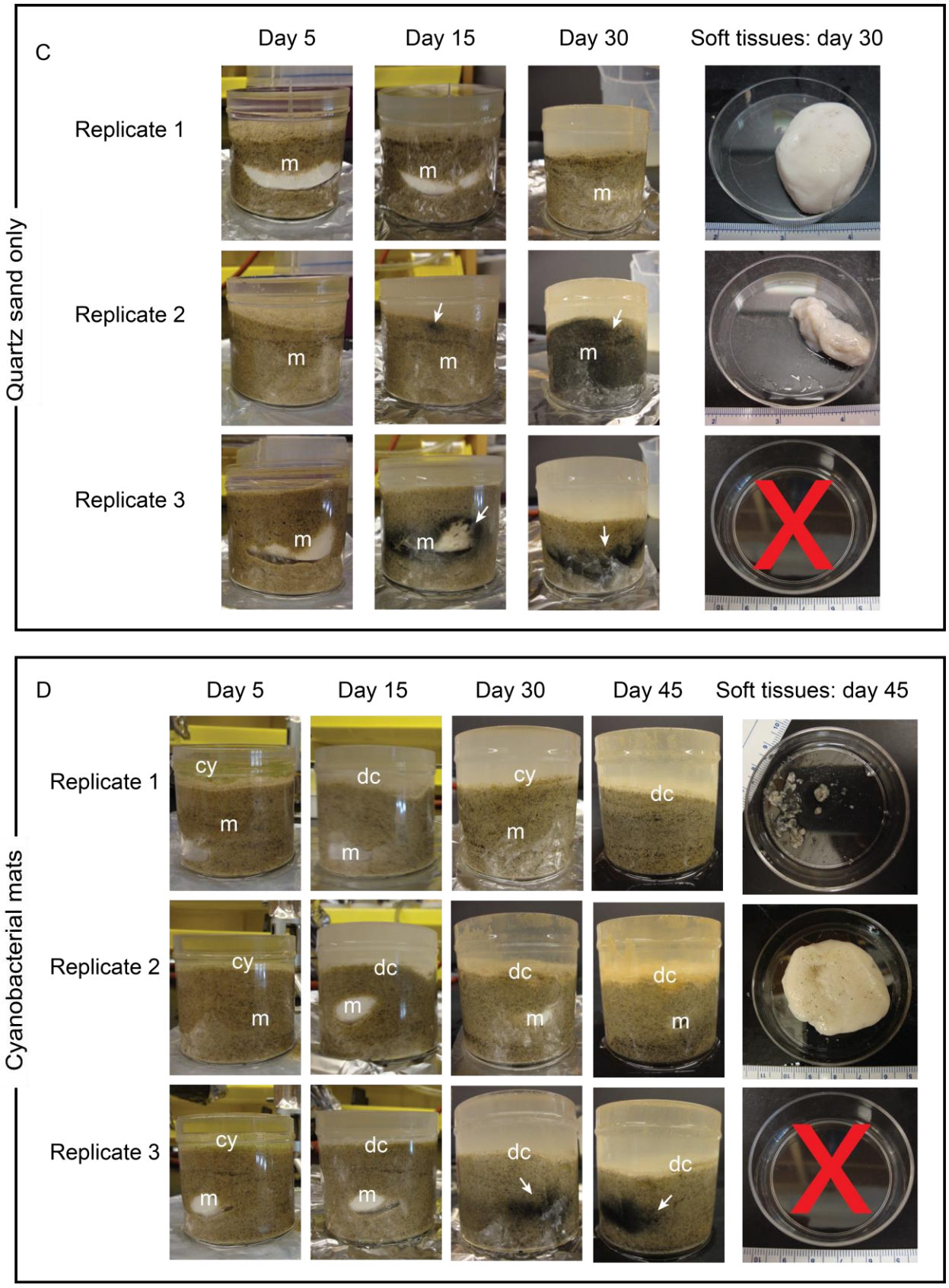
C
Day 5
Day 15
Day 30
Soft tissues: day 30
Quartz sand only
Replicate 1
Replicate 2
Replicate 3
m
D
Day 5
Day 15
Day 30
Day 45
Soft tissues: day 45
Cyanobacterial mats
Replicate 1
Replicate 2
Replicate 3
cy
dc
m

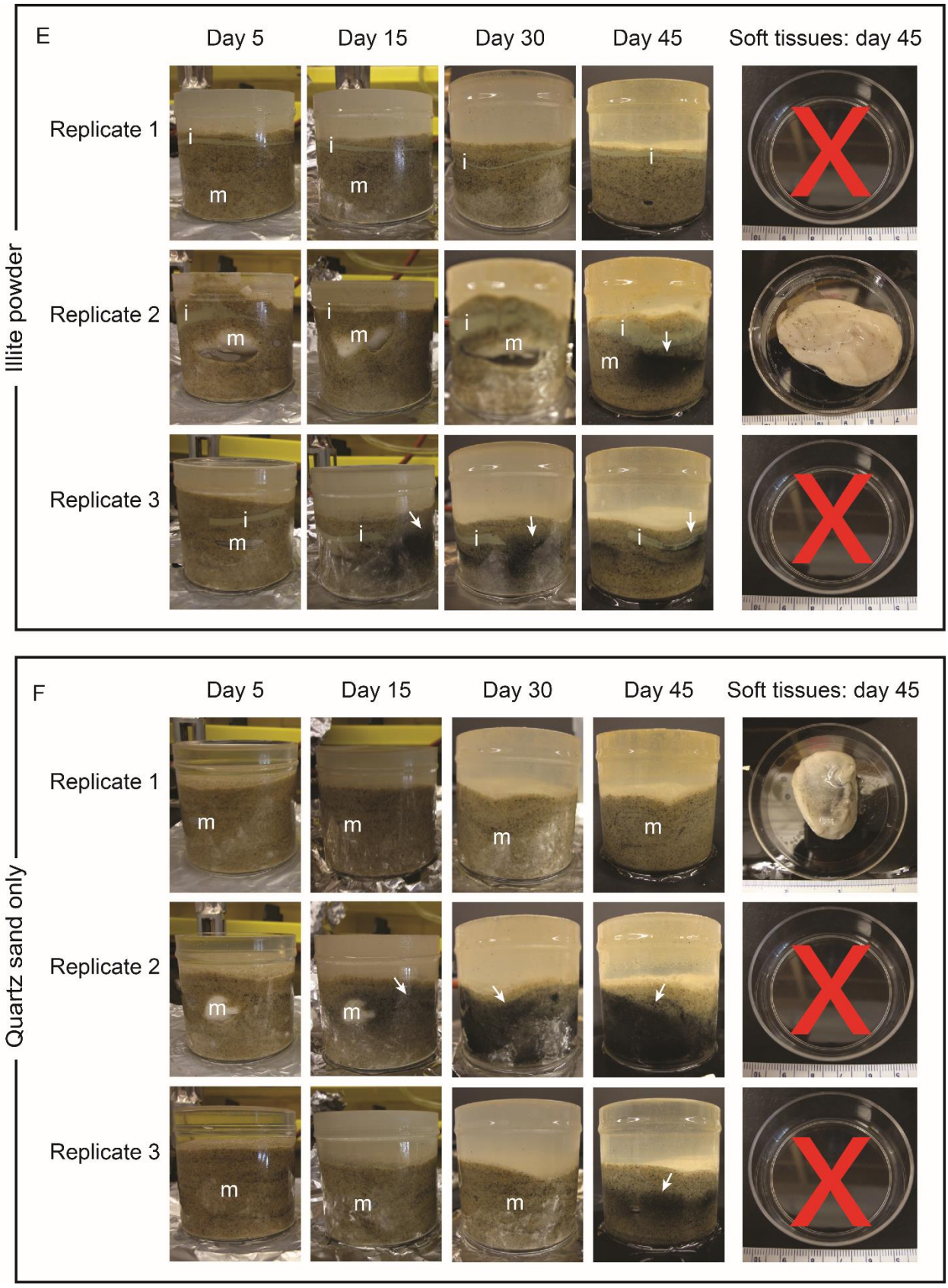
E
Day 5
Day 15
Day 30
Day 45
Soft tissues: day 45
Illite powder
Replicate 1
Replicate 2
Replicate 3
i
m
F
Quartz sand only

SUPPLEMETARY FIGURE 2.–Photographs of muscles at different time points (1, 5, 15, 30 and 45 days) and specimens exhumed from the sand on day 30 or 45. Photographs of exhumed muscles are to the right of corresponding time series photographs. Muscles buried in quartz sand for 30 days: **A)** Muscle incubated in the presence of cyanobacterial cells. **B)** Muscle incubated in the presence of illite. **C)** Muscle incubated without added cyanobacteria/clay minerals. Muscles buried in quartz sand for 45 days: **D)** Muscle incubated in the presence of cyanobacteria. **E)** Muscle incubated in the presence of illite. **F)** Muscle incubated without added cyanobacteria/clay minerals. Culture jar volume is 190 mL; solid arrows indicate extensive black patches around muscles. *m* = muscle tissue; *cy* = living cyanobacterial cells; *dc* = dead cyanobacterial cells; *X*= the complete decay of soft tissues by the end of the experiment.

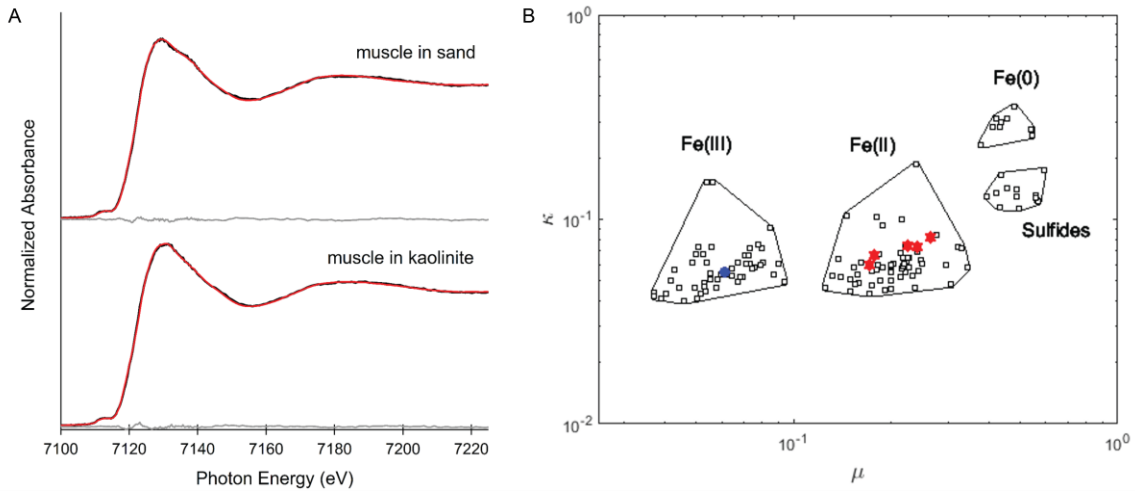

SUPPLEMENTARY FIGURE 3.–Representative Fe K-edge XANES spectra for muscles exhumed from sand and kaolinite and scatterplot comparing normalized absorption values of muscle tissues and sterile kaolinite. **A)** Fe XANES spectra for the muscles exhumed from sand and kaolinite after 45 days of burial. The spectra are derived from individual XANES spots (spots four and five in Fig. 4B and C, respectively). The best least-square linear combination fits for the muscles exhumed from sand and kaolinite are shown in red (sand: 58.9% Fe(II) sulfate, 39.8% goethite, sum-sq: $3.3x10^{-4}$; kaolinite: 37.8% Fe-rich basaltic glass, 22.0% ferrosmectite and 20.2% kaolinite, sum-sq: $9.9x10^{-5}$) and the residual for both is plotted in gray. **B)** Scatterplot of the normalized Fe K-edge XANES absorption values at 7117.5 eV and 7113 eV (a versus b, respectively). Black empty squares = Fe-bearing minerals or chemical standard compounds of known Fe valence; blue circles = sterile kaolinite (average of four XANES spots); red stars = muscle exhumed from kaolinite (five XANES spots).

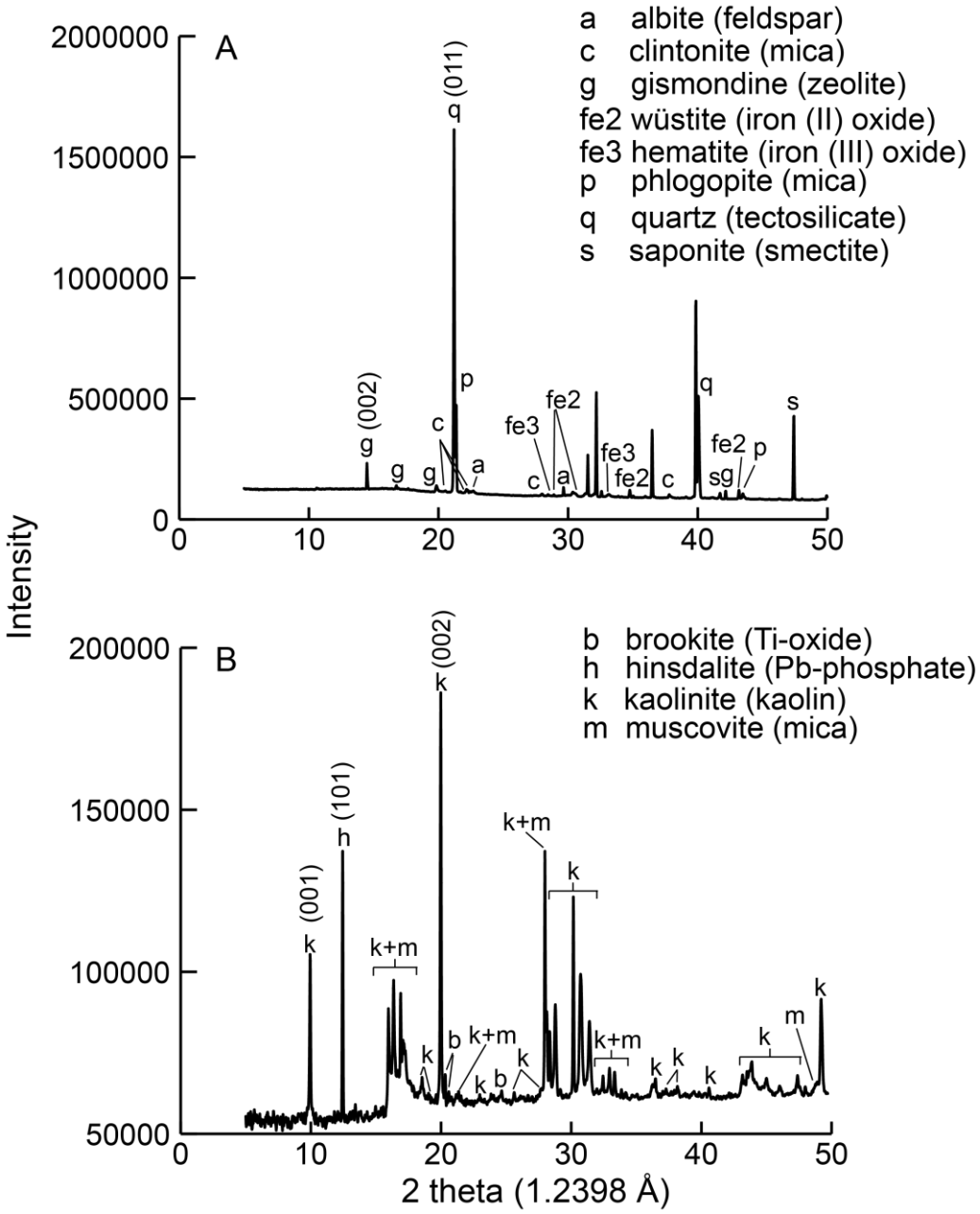

SUPPLEMENTARY FIGURE 4.–Micro-XRD spectra of sterile substrates in the absence of muscle tissues. **A)** Sterile sand is composed of albite, clintonite, gismondine, wüstite, hematite, phlogopite, quartz and saponite. **B)** Sterile kaolinite is composed of kaolinite grains, as well as impurities such as muscovite, brookite and an Pb-rich mineral (possibly hinsdalite). See Supplementary Fig. 7 for SEM-EDS results for the Pb-rich mineral found in the sterile kaolinite.

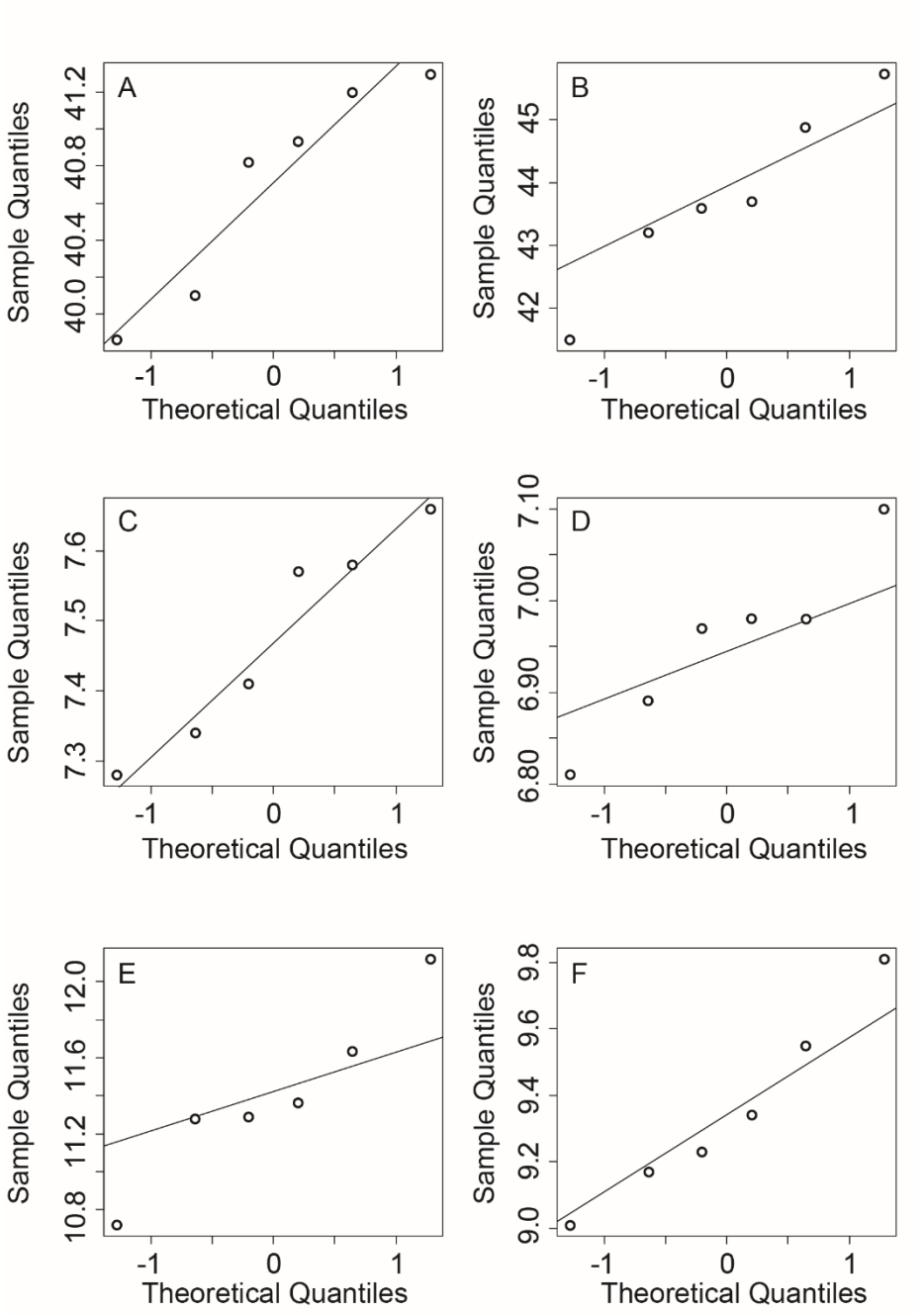

SUPPLEMENTARY FIGURE 5.–Normal quantile-quantile plots of carbon, hydrogen and nitrogen content (%) of muscles. The left column shows samples before and the right column shows samples after 45 days of incubation in kaolinite. **A)** Carbon content of muscles before experimentation. **B)** Carbon content of muscles after burial. **C)** Hydrogen content of muscles before experimentation. **D)** Hydrogen content of muscles after burial. **E)** Nitrogen content of muscles before experimentation. **F)** Nitrogen content of muscles after burial.

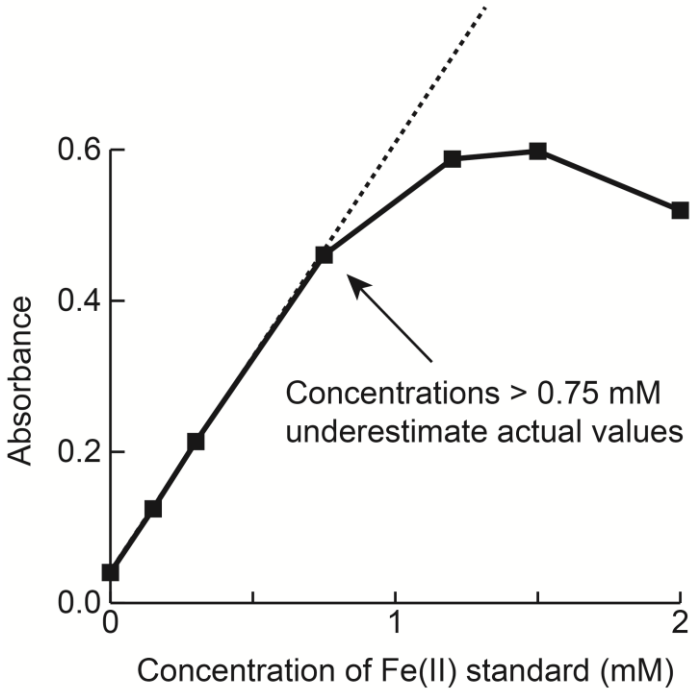

SUPPLEMENTARY FIGURE 6.–Testing the effect of sample dilution after the addition of ferrozine on the measured concentrations of Fe(II). Standards were diluted 20x after the addition of ferrozine and measured using colorimetric assays. Concentrations of Fe(II) that were originally greater than 0.75 mM were underestimated. Solid line shows absorbance values for diluted standards; dashed line shows calculated absorbance values based on the known added concentrations of standards.

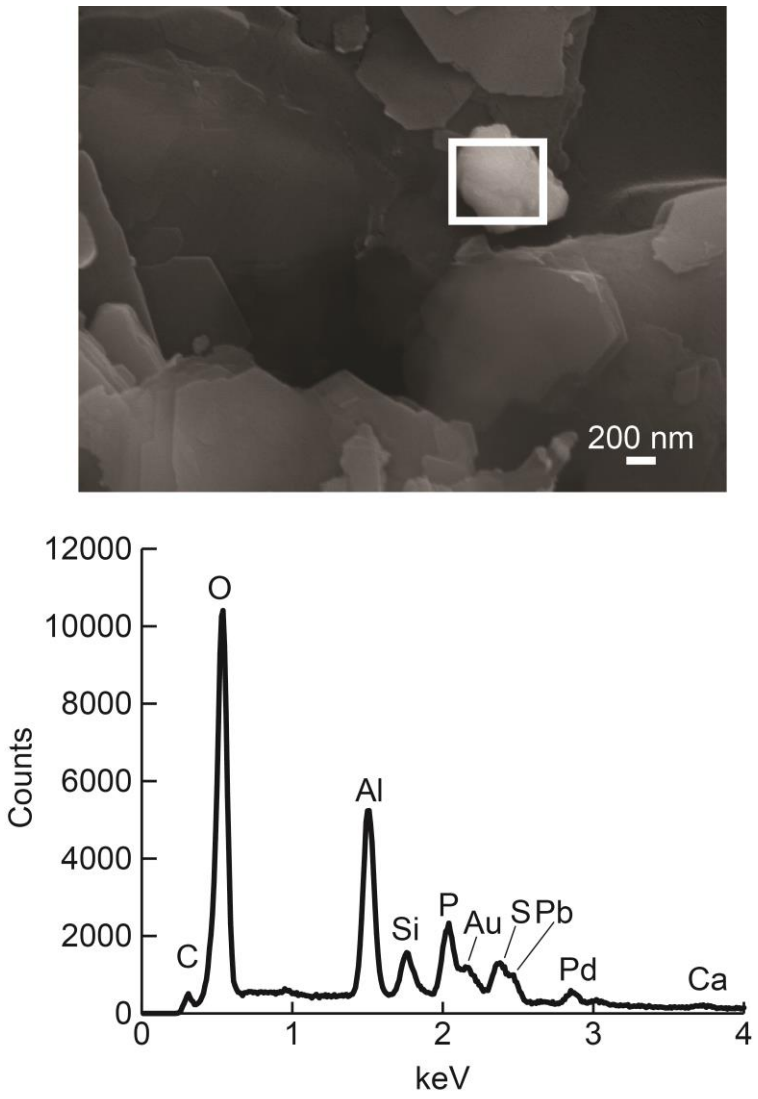

SUPPLEMENTARY FIGURE 7.– Representative scanning electron micrograph (SEM) and energy dispersive X-ray spectra (EDS) of Pb-rich mineral found in the sterile kaolinite substrate. Sample was coated with gold and palladium. White box shows area analyzed by SEM-EDS and corresponding EDS spectrum is found below the SEM micrograph.

SUPPLEMENTARY TABLE 1.–List of best fit Fe standards

Substrate	Microbes or clay added?	Day exhumed	XANES spot number	Minerals identified	Amounts (%)	Sum-square	Sum-absolute value
sand	cyanobacteria	30	1	FeS (synthetic)	13.5	1.96E-04	1.27E-02
			1	Fe(II) sulfate	55.9		
			1	goethite	29.8		
			2	FeS (synthetic)	14.7	1.98E-04	1.31E-02
			2	Fe(II) sulfate	56.5		
			2	goethite	28.2		
			3	Fe(II) phosphate	41.1	2.59E-04	1.47E-02
			3	pyrite	12.1		
			3	iron oxyhydroxide*	46.7		
sand	cyanobacteria	30	1	Fe(II) sulfate	51.8	1.51E-04	1.13E-02
			1	goethite	10.6		
			1	siderite	36.8		
			2	seafloor basalt**	53.2	2.30E-04	1.34E-02
			2	Fe(II) sulfate	18.2		
			2	iron oxyhydroxide*	28.6		
sand	cyanobacteria	45	1	Fe(II) sulfate	48.2	2.E7E-04	1.36E-02
			1	goethite	50.1		
			2	Fe(II) sulfate	58.8	2.11E-04	1.29E-02
			2	goethite	39.4		
			3	Fe(II) sulfate	52.1	2.04E-04	1.26E-02
			3	goethite	46.3		
			4	Fe(II) sulfate	55.2	2.03E-04	1.30E-02
			4	iron oxyhydroxide*	43.8		
sand	none	30	1	seafloor basalt**	12.2	9.22E-05	8.22E-03
			1	Fe(II) sulfate	59.0		
			1	goethite	27.9		
			2	Fe(II) sulfate	68.0	1.61E-04	1.19E-02
			2	jarosite	30.9		

			3	Fe(II) sulfate	60.6	1.12E-04	8.68E-03
			3	goethite	38.8		
			4	Fe(II) sulfate	61.8	1.31E-04	9.76E-03
			4	goethite	37.6		
			5	Fe(II) sulfate	63.0	1.76E-04	1.14E-02
			5	goethite	36.2		
			6	Fe(II) sulfate	56.1	1.73E-04	1.16E-02
			6	goethite	43.3		
sand	none	45	1	Fe(III) alginate	44.3	2.84E-04	1.30E-02
			1	Fe(II) sulfate	54.7		
			2	ferrihydrite	36.2	3.58E-04	1.51E-02
			2	Fe(II) sulfate	62.2		
			3	Fe(II) sulfate	65.0	4.53E-04	1.66E-02
			3	goethite	33.4		
			4	Fe(II) sulfate	58.9	3.33E-04	1.45E-02
			4	goethite	39.8		
			5	Fe(III) alginate	35.5	6.78E-05	7.25E-03
			5	Fe(II) sulfate	52.6		
			5	goethite	43.3		
sand	none	45	1	Fe(III) alginate	17.2	1.33E-04	1.04E-02
			1	Fe(II) sulfate	55.4		
			1	pyrite	26.9		
			2	Fe(II) sulfate	65.1	1.47E-04	1.09E-02
			2	pyrite	16.4		
			2	iron oxyhydroxide*	17.9		
			3	seafloor basalt**	34.0	1.08E-04	8.94E-03
			3	Fe(II) sulfate	46.2		
			3	goethite	19.2		
			4	Fe(III) alginate	21.8	1.10E-04	9.49E-03
			4	Fe(II) sulfate	62.6		
			4	pyrite	15.0		
			5	Fe(II) sulfate	63.9	1.09E-04	9.82E-03

			5	pseudobrookite	17		
kaolinite	n/a	45	1	seafloor basalt**	64.5	1.73E-04	1.12E-02
			1	smectite	35.6		
			2	seafloor basalt**	75.4	2.85E-04	1.44E-02
			2	smectite	23.9		
			3	seafloor basalt**	45.3	1.27E-4	1.01E-02
			3	kaolinite	54.7		
			4	seafloor basalt**	28.5	5.01E-05	6.12E-03
			4	Fe(II) sulfate	33.1		
			4	kaolinite	37.8		
			5	seafloor basalt**	37.8	9.90E-5	8.44E-03
			5	ferrosmectite	22.0		
			5	kaolinite	20.2		

Note: Dashed lines separate individual muscle specimens. Spectra were least-square linear combination fitted using a large database of Fe-bearing standard compounds. Several XANES spot analyses were taken for each specimen and these spots were numbered incrementally, starting with spot one.

*Reference: Toner B., Santelli C.M., Marcus M.A., Wirth R., Chan C.S., McCollum T., Bach W., Edwards K.J., 2009, Biogenic iron oxyhydroxide formation at mid-ocean ridge hydrothermal vents: Juan de Fuca Ridge: Geochimica et Cosmochimica Acta, v. 73, p. 388-403.

**An unidentifiable, likely amorphous and silica-rich phase in the veneers that did not match with any of the iron standards. Reference for the seafloor basalt standard: Santelli, C., Geomicrobiology of the ocean crust: The phylogenetic diversity, abundance, and distribution of microbial communities inhabiting basalt and implications for rock alteration processes: Unpublished Ph.D. thesis, MIT/WHOI Joint Program in Oceanography, Woods Hole, 217 p.

SUPPLEMENTARY TABLE 2.– Time series of porewater chemistry measurements in kaolinite/quartz sand with buried muscle tissues and sterile control experiments without any tissues.

		Muscles incubated in clay/sand						Sterile experiments, no muscles			
Day	Ions/dissolved silica/pH	Quartz sand			Kaolinite			Quartz sand		Kaolinite	
		R1	R2[ɪ]	R3	R1[ɪ]	R2[ɪ]	R3	R1	R2	R1	R2
10	silica (mM)	2.39	1.48	0.40	1.28	1.32	1.71	0.45	0.39	0.46	0.62
	Fe^{2+} (mM)	>1.14*	0.34*	>1.17*	0.17	0.20	0.14	<0.01	<0.01	n.d.	n.d.
	Fe^{3+} (mM)	>0.24*	>0.16*	>0.27*	0.16	>0.06*	>0.03*	<0.01	<0.01	<0.01	<0.01
	sulfide (µM)	1.22	6.53	37.99	0.02	n.d.	n.d.	n.d.	n.d.	0.29	n.d.
	pH	--	--	--	--	--	--	7.0	7.0	7.0	7.0
15	silica (mM)	--	--	--	--	--	--	0.48	0.41	0.65	0.64
	Fe^{2+} (mM)	>1.0*	0.13	>1.04*	0.05	0.11	0.15	<0.01	<0.01	<0.01	n.d.
	Fe^{3+} (mM)	>0.11*	0.24	>0.14*	0.13	>0.01*	0.13	<0.01	<0.01	<0.01	<0.01
	sulfide (µM)	1.82	3.92	10.34	1.05	2.59	n.d.	n.d.	n.d.	n.d.	n.d.
	pH	4.5	6.5	5.5	6.5	6.5	6.0	7.0	7.0	7.0	7.0
20	silica (mM)	2.01	0.72	1.70	1.45	1.10	0.96	0.27	0.29	0.36	0.38
	pH	5.5	7.0	5.5	7.0	7.0	7.0	7.0	7.0	7.0	7.0
30	silica (mM)	0.39	0.45	1.30	0.35	0.65	0.52	0.23	0.42	0.30	0.51
	Fe^{2+} (mM)	0.03	0.02	0.80**	<0.01	<0.01	0.01	<0.01	<0.01	n.d.	<0.01
	Fe^{3+} (mM)	0.08	0.15	0.32**	0.01	0.06	0.05	<0.01	<0.01	<0.01	<0.01
	sulfide (µM)	n.d.	1.39	1.61	n.d.	n.d.	0.06	n.d.	0.24	0.29	n.d.
	pH	6.5	7.0	6.0	7.0	6.5	6.5	7.0	7.0	7.0	7.0
45	silica (mM)	0.60	0.67	1.12	1.16	0.77	0.93	0.28	0.35	0.45	0.45
	Fe^{2+} (mM)	0.01	<0.01	0.02	0.03*	<0.01	<0.01	<0.01	n.d.	n.d.	n.d.
	Fe^{3+} (mM)	0.14	0.16	0.36	>0.05*	0.04	0.03	<0.01	<0.01	<0.01	<0.01
	sulfide (µM)	n.d.	n.d.	1.95	n.d.	n.d.	n.d.	n.d.	0.39	0.10	0.34
	pH	7.0	7.5	7.5	7.5	7.5	7.0	7.0	7.0	7.0	7.0

Note: *R1-R3* denotes replicate experiments one through three and *n.d.* denotes below the limit of detection.

[ɪ]Sample was successfully recovered on day 45.

*Sample was diluted 20x in 0.1 M NaCl water *after* the addition of ferrozine.

**Sample was diluted 20x in 0.1 M NaCl water *before* the addition of ferrozine.

SUPPLEMENTARY TABLE 3.– Porewater pH values in sand that contained cyanobacteria/illite and muscle tissues. The corresponding control experiments contained tissues, but did not contain cyanobacteria/illite.

	Cyanobacteria						Illite						Quartz sand only					
Day	R1		R2		R3		R1		R2		R3		R1		R2		R3	
	PW1	PW2	PW1*	PW2ǂ	PW1	PW2	PW1	PW2	PW1*	PW2ǂ	PW1	PW2	PW1*	PW2ǂ	PW1	PW2	PW1	PW2
10	6.0	6.0	6.0	6.2	5.7	5.9	5.9	6.1	6.2	6.1	6.0	6.0	5.7	6.1	6.3	6.0	6.0	6.2
15	6.1	5.5	6.8	5.8	5.4	5.4	6.3	6.4	6.1	5.9	6.4	6.2	5.2	6.0	6.2	6.4	6.2	6.5
20	6.4	5.4	5.7	7.0	5.6	5.4	6.8	6.5	6.6	6.2	6.6	6.7	5.0	6.2	6.9	6.9	6.5	6.7
25	6.5	5.9	6.4	6.0	6.0	5.6	6.7	7.0	6.7	6.2	6.9	6.8	4.9	6.4	7.2	7.0	6.6	6.8
30	6.7	6.2	6.4	6.9	6.6	6.4	6.6	7.0	6.9	6.5	6.8	6.9	5.1	6.7	7.3	--	6.7	7.0
40	--	6.6	--	6.8	--	6.4	--	6.9	--	6.7	--	6.9	--	6.7	--	7.3	--	6.6
45	--	6.8	--	6.6	--	6.5	--	7.0	--	6.9	--	7.1	--	6.8	--	7.2	--	7.0

Note: *R1-R3* denote replicate experiments one through three; *PW1* and *PW2* denote pore fluids one and two, respectively. Muscles were exhumed from PW1 on day 30 and PW2 on day 45.

*Intact muscle was recovered on day 30.

ǂIntact muscle was recovered on day 45.